Nanoscale Research Letters

NANO EXPRESS

Structural Features of Carbons Produced Using Glucose, Lactose, and Saccharose

Ivan F. Myronyuk[1], Volodymyr I. Mandzyuk[1*], Volodymyr M. Sachko[1] and Volodymyr M. Gun'ko[2]

Abstract

Glucose, lactose, and saccharose were used as precursors to prepare chars at 400 °C then activated at 800 °C or 1000 °C in closed vessels with controlled amounts of oxygen penetrating through nanopores in the vessel walls. There are correlations between the porosity, amounts of residual O- and H-containing functionalities, and electroconductivity of amorphous carbons studied. The pore size distributions calculated using the nitrogen adsorption isotherms and TEM images show that all carbons are mainly nanoporous with certain contribution of narrow mesopores (at pore half-width $x < 5$ nm). Oxidizing activation by oxygen penetrating into the closed vessels with chars through nanopores can more strongly change the outer layers of char particles than the inner pores. Therefore, despite relatively great burn-off degree, the textural characteristics are relatively low for activated carbons.

Keywords: Activated carbons, Thermal degradation processes, Porous structure, surface functional groups, Specific conductivity

PACS: 81.05.Rm, 81.05.Uw, 87.14.Df

Background

Carbons are frequently produced using natural row materials, which include carbohydrates [1–13]. Carbohydrates (e.g., saccharides) are appropriate materials for carbonization because they include many well-removed O/H-containing functionalities [14–25]. Therefore, their carbonization with the dehydration as one of the main processes can be carried out at temperatures (320–500 °C) lower than that used for carbonization of other compounds, e.g., phenolformaldehyde resin at 800 °C [26–28]. To improve the textural characteristics of chars, they are activated in the atmosphere with water vapor, CO_2, or CO at 800–1100 °C [1–3, 29]. Carbonization of precursors mixed with such active compounds as zinc chloride, phosphorus acid, and potassium carbonate can provide a high porosity of the carbons without of additional activation [30–32].

The physicochemical properties of the carbonaceous materials depend strongly on the characteristics of their precursors. Since chars are composed of polyaromatic structures (graphenes), the presence of cyclic fragments in the precursors is favorable for effective carbonization. Therefore, thermolysis of mono- or disaccharides results in the formation of polyaromatic compounds, whose condensation gives graphene clusters. Among simple carbohydrates, saccharose is frequently used as a char precursor [13–25, 33–35]. Mono- and disaccharides are characterized by tautomerism and diastereoisomerism, e.g., besides chain-cyclic tautomerism of glucose, there are eight pairs of its diastereomers. The tautomers and diastereomers (stereoisomers not related as mirror images) are characterized by different physicochemical properties [36, 37]. This can affect the carbonization results for saccharides. Note that carbonization of glucose or other small organic molecules at a surface of oxide materials (such as silica gels, fumed silica, titania, and mixed oxides) typically results in the formation of nonporous carbon nanoparticles similar to those of carbon black [38, 39]. Besides dependences of the textural characteristics of chars on the structure of different saccharides used as precursors, there is an additional question on the effects of activation of chars by small controlled portions of oxygen. Therefore, the aim of this work was to study the thermolysis of glucose (as a

* Correspondence: mandzyuk_vova@ukr.net
[1]Vasyl Stefanyk Precarpathian National University, 57 Shevchenko Street, 76018 Ivano-Frankivsk, Ukraine
Full list of author information is available at the end of the article

Myronyuk *et al. Nanoscale Research Letters* (2016) 11:508

Page 2 of 9

monosaccharide) and two disaccharides (such as lactose composed of β-D-galactopyranose and α-D-glucopyranose and saccharose composed of α-D-glucopyranose and β-D-fructofuranose), and the characteristics of the chars (carbonized at 400 °C) and related carbons activated at 800 and 1000 °C using controlled amounts of oxygen.

Methods

Crystalline monohydrates of glucose, lactose, and anhydrous saccharose were used as precursors of chars prepared at 400 °C for 30 min in air. Oxidizing activation of chars was carried out in ceramic crucibles at 800 or 1000 °C for 30 min. Oxygen (from air) penetrated into the crucibles through mesoporous walls (porosity ~20%). The pore sizes in the walls were decreased by fourfold to fivefold impregnation with a concentrated solution of $AlONO_3 \cdot 2H_2O$, dried, and then calcined at 800 °C. Mesoporous alumina filling macropores of the crucible walls has pores of approximately 5 nm in size. Caps of the crucibles were sealed using asbestos strings.

Thermal degradation of glucose, lactose, and saccharose in 25–1000 °C range was studied using thermogravimetry (TG) with a STA 449 F3 Jupiter (Netzsch) apparatus at a heating rate of 5 °C/min in the inert (argon) atmosphere.

The textural characteristics of chars and activated carbons, AC (degassed at 180 °C for 24 h), have been determined using the nitrogen adsorption-desorption isotherms recorded at 77.4 K using a Quantachrome Autosorb Nova 2200e adsorption analyzer. The pore size distributions (PSDs) (differential $\sim dV/dx$) have been calculated using the quenched solid density functional theory (QSDFT, Quantachrome software) [40] and 2D-nonlocal DFT (2D-NLDFT, SAIEUS program, Micromeritics software) [41, 42] methods with the slit-shaped pore model. Additionally, the complex model with slit-shaped (S) and cylindrical (C) pores and voids (V) between nanoparticles (SCV-model) with self-consisting regularization (SCR) procedure was used [43]. The differential PSD functions with respect to the pore volume (PSD$_V$, $f_V(x) \sim dV/dx$, $\int f_V(x)dx \sim V_p$) and the specific surface area (PSD$_S$, $f_S(x) \sim dS/dx$, $\int f_S(x)dx \sim S$) were used to estimate the contribution of nano- ($x < 1$ nm), meso- ($1 < x < 25$ nm), and macropores ($x > 25$ nm).

The X-ray diffraction (XRD) patterns of samples treated at different temperatures were recorded at room temperature using a DRON-4-07 (Burevestnik, St. Petersburg) diffractometer with Cu K$_\alpha$ ($\lambda = 0.154178$ nm) radiation and a Ni filter in the 2θ range from 10° to 65° with a step of 0.1° using the Bragg-Brentano geometry.

Infrared (IR) spectra were recorded using a Specord M80 spectrometer over the 400–4000 cm^{-1} range. A sample (4 mg) was stirred with dry KBr (weight ratio 1:100), treated in a stainless steel microbreaker for 10 min, and pressed in a thin transparent plate of 20×5 mm^2 in size.

Transmission electron microscopy (TEM) images have been obtained using a JEOL JSM-2100F field emission TEM operated at 200 kV. TEM images have been analyzed using Fiji (local thickness plugin) [44] and ImageJ (granulometry plugin) [45, 46] software.

Desorption of fragments with C$_4$, C$_5$, C$_6$, and C$_9$, as well as CO, CO$_2$, and others, was analyzed using temperature-programmed desorption (TPD) with mass-spectroscopic (MS) control using a MX 7304A mass spectrometer
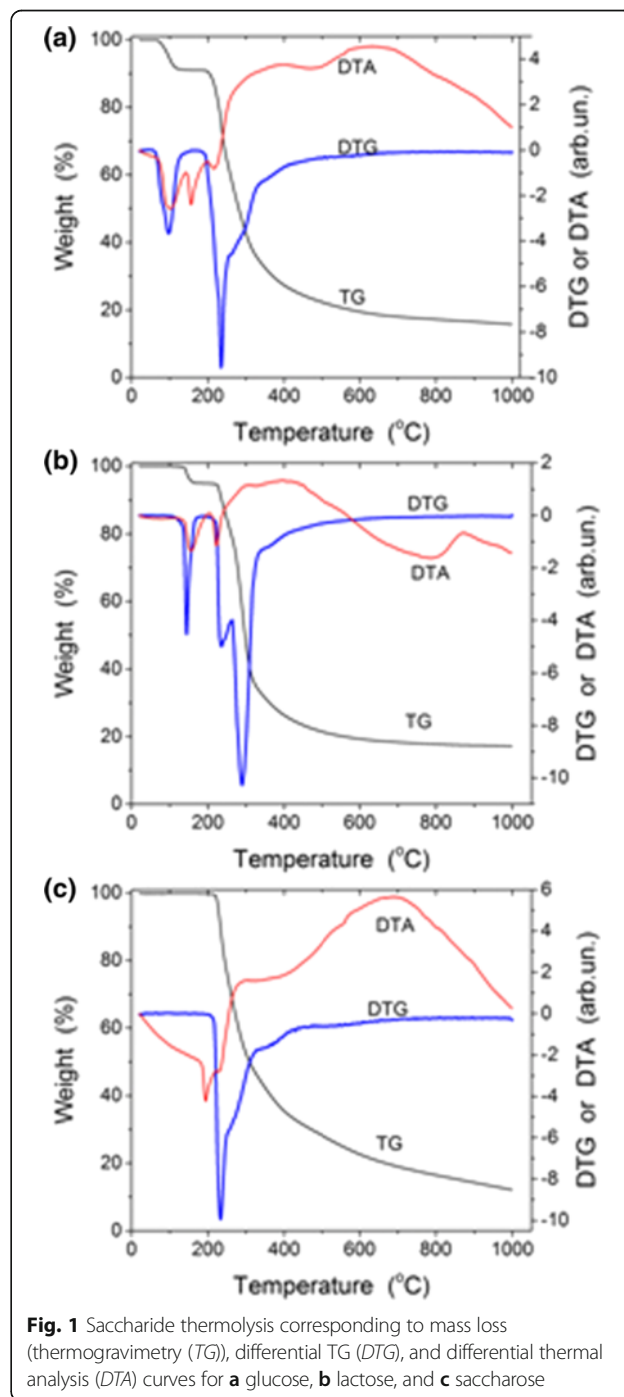

Fig. 1 Saccharide thermolysis corresponding to mass loss (thermogravimetry (*TG*)), differential TG (*DTG*), and differential thermal analysis (*DTA*) curves for **a** glucose, **b** lactose, and **c** saccharose

Myronyuk *et al. Nanoscale Research Letters* (2016) 11:508

Page 3 of 9

(Electron, Sumy, Ukraine, sensitivity ~10^{-8} g at m/z 1–400) [47, 48]. A sample (~4 mg) placed in a quartz–molybdenum cell (diameter 11 mm) was degassed at room temperature and pressure 7×10^{-5} Pa and then heated to 800 °C at a linear heating rate of 1 °C/min. Volatile products are desorbed from the sample, ionized by the electron beam, separated by a mass-analyzer, and brought to a detector.

Impedance analysis of carbon samples was carried out using a Metrohm Autolab FRA-2 (Frequency Response Analyzer) at 10^{-2}–10^{5} Hz and voltage amplitude of 10 mV [49].

Results and Discussion

The thermolysis of glucose, lactose, and saccharose in the inert atmosphere (Fig. 1, Table 1) shows several processes: desorption of intact water (65–145 °C for glucose and 100–175 °C for lactose as crystalline hydrates), melting, caramelization, dehydration (associative desorption of water molecules), carbonization (formation of polyaromatics and carbon sheets and graphenes), and structure transformation of chars.

The maximal rate of removal of intact water is at 96 °C for glucose and 144 °C for lactose (Fig. 1a, b, DTG). The processes of water removal, caramelization (~160 °C), melting (160, 220, and 197 °C for glucose, lactose, and saccharose, respectively), and dehydration are endothermic ones (Fig. 1, DTA minima). Removal of water due to the condensation reactions between the hydroxyl groups of interacting molecules and the formation of polyaromatic

compounds occur at 200–330 °C (glucose), 230–355 °C (lactose), and 218–345 °C (saccharose). These processes result in the mass loss (Table 1). The residual mass corresponds to 40% (glucose and lactose) and 42% (saccharose) with respect to the initial precursor mass. This corresponds to the loss of a major fraction of structural water due to
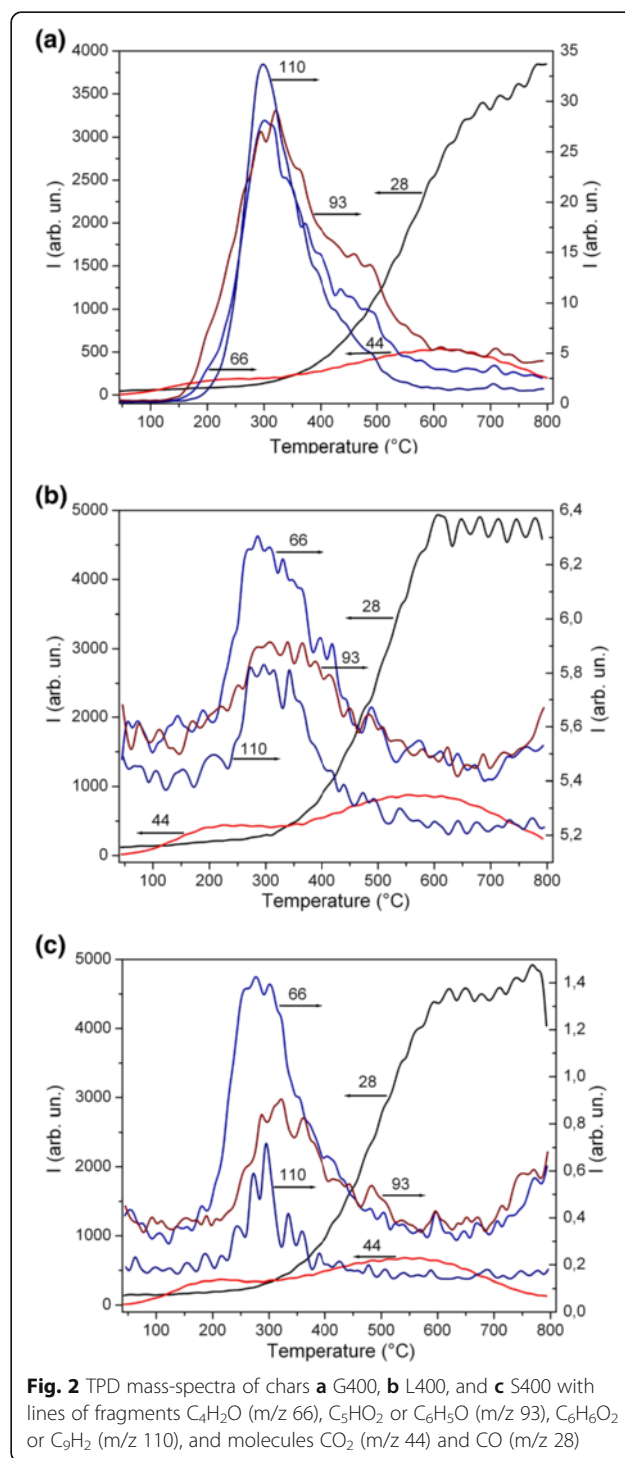
Table 1 Processes observed during heating of precursors to 1000 °C

Processes	Glucose	Saccharose	Lactose
	$C_6H_{12}O_6 \cdot H_2O$	$C_{12}H_{22}O_{12}$	$C_{12}H_{22}O_{11} \cdot H_2O$
Intact water removal			
Temperature (°C)	65–145	–	100–175
Water loss (mole)	1	–	1
Melting			
Temperature (°C)	160	197	220
Dehydration			
Temperature (°C)	200–230	218–260	220–230
Water loss (mole)	1	5	3
Carbonization			
Temperature (°C)	230–332	260–355	230–343
Water loss (mole)	5	6	8
Residual mass (%)	40	42	40
Char structure changes			
Temperature (°C)	332–1000	355–1000	343–1000
Residual mass (%)	16	12	17
Mass loss in this process (%)	60	75	55

Fig. 2 TPD mass-spectra of chars **a** G400, **b** L400, and **c** S400 with lines of fragments C_4H_2O (m/z 66), C_5HO_2 or C_6H_5O (m/z 93), $C_6H_6O_2$ or C_9H_2 (m/z 110), and molecules CO_2 (m/z 44) and CO (m/z 28)

Myronyuk *et al. Nanoscale Research Letters* (2016) 11:508

Page 4 of 9

condensation of O-containing functionalities. Subsequent heating to 1000 °C leads to the mass loss up to 88% (saccharose), 84.3% (glucose), and 82.9% (lactose). Residual carbon remains because the process was carried out in the inert atmosphere.

The most intensive lines in the TPDMS thermograms of chars correspond to the elimination of CO and CO_2 (Fig. 2). This suggests that the residual amounts of O-containing functionalities in the chars are relatively great. Certain amounts of H-containing functionalities should be remained in the chars. These results are in agreement with the IR spectra of L400 (Fig. 3) showing the presence both C–H (bands at 2924–2916 and 2868 cm^{-1}) and O–H (a broad band at 3450 cm^{-1}) functionalities in the chars. The maximal amounts of desorbed fragments (such as C_4H_2O at m/z 66, C_5HO_2 or C_6H_5O at m/z 93, and $C_6H_6O_2$ or C_9H_2 at m/z 110) are observed at ~300 °C (mainly in the range of 200–500 °C, Fig. 2). However, CO elimination is maximal at 600–800 °C that corresponds to structural changes in the chars observed in the TG/DTG/DTA thermograms at high temperatures (Fig. 1).

Carbonization of a melted precursor is accompanied by elimination of water vapor that results in boiling up of the reacted precursor. This provides the formation of pores in the chars. The chars and AC have a lamellar shape (Fig. 4b, d) with a stack thickness of 5–40 nm. Nanosized graphenes (1–5 nm in size) form a random amorphous structure of the carbons (Fig. 4a, c). The XRD patterns of lactose-based char and carbons (Fig. 5) and electron diffraction patterns (see Additional file 1: Figure S1) confirm that the materials are amorphous.

The most nitrogen adsorption-desorption isotherms of the carbons studied are characterized by open hysteresis loops (Fig. 6). This can be due to the presence of long and narrow pores with narrow necks close in size to the nitrogen molecules [50]. As a whole, all samples are nanoporous with a certain contribution of narrow mesopores (Table 2, Figs. 7 and 8, and in Additional file 1: Figure S2). Note that the G400 sample was with very low open porosity; therefore, the nitrogen adsorption isotherm was not recorded. However, this sample has certain closed porosity because the specific surface area estimated from the SAXS data corresponds to 185 m^2/g (the procedure of SAXS investigation is described in detail in [51]).

An increase in the activation temperature from 800 to 1000 °C for lactose- and saccharose-based chars leads to the enhancement of the porosity (Table 2, V_p, S_{BET}). However, direction of changes in the PSD is opposite for these samples with increasing temperature (Fig. 7), and the effect is much smaller for saccharose-based carbons.

Note that the SCV/SCR method gives slightly broader PSD (see Additional file 1: Figure S2) than the 2D-NLDFT or QSDFT methods with the slit-shaped pore model (Figs. 7 and 8). However, the PSDs based on the TEM images (Fig. 8) show the presence of narrow mesopores similar to that of the SCV/SCR PSD. Therefore, the textural characteristics shown in Table 2 are based on the SCV/SCR results.

The XRD patterns are shown only for lactose-based carbons (Fig. 5) as representative materials (other carbons have similar XRD patterns). For L400, there is the main line at 2θ = 22° and a weak features at 43°. The second XRD reflection is much intensive for L800 (23° and 43°) and L1000 (24.2° and 43.6°). The inter-plate distances estimated from these values correspond to 0.404 and 0.199 nm (L800) and 0.367 and 0.207 nm (L1000). For
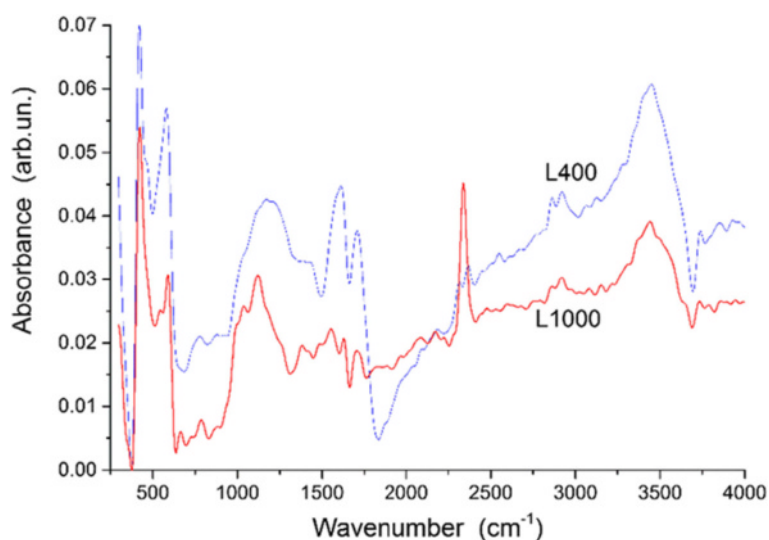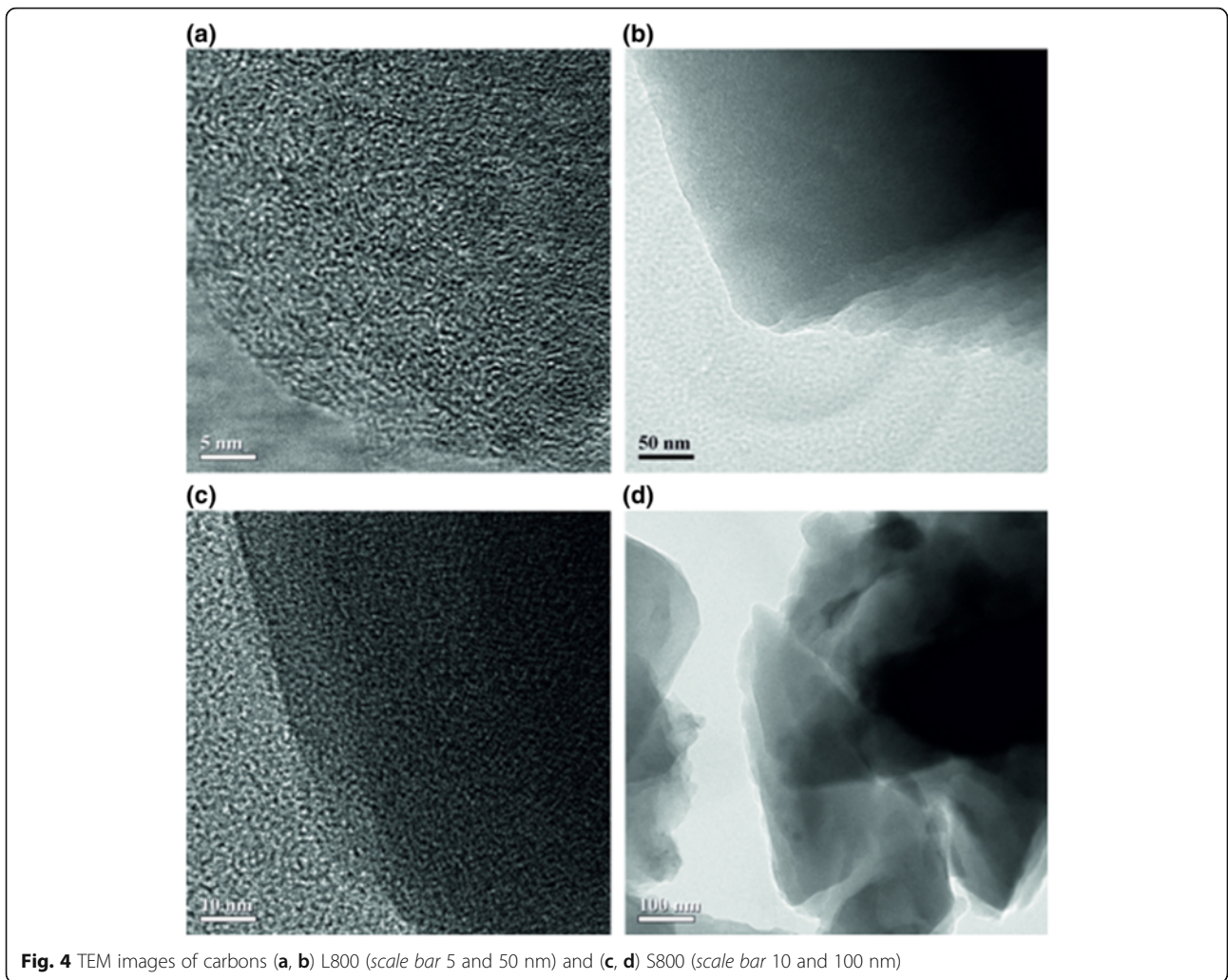

Fig. 3 IR spectra of samples L400 and L1000

Myronyuk *et al. Nanoscale Research Letters* (2016) 11:508

Page 5 of 9

Fig. 4 TEM images of carbons (**a**, **b**) L800 (*scale bar* 5 and 50 nm) and (**c**, **d**) S800 (*scale bar* 10 and 100 nm)

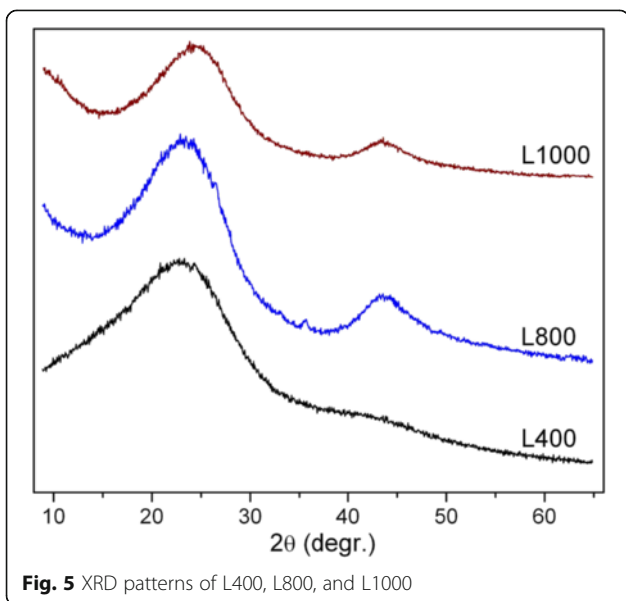**Fig. 5** XRD patterns of L400, L800, and L1000
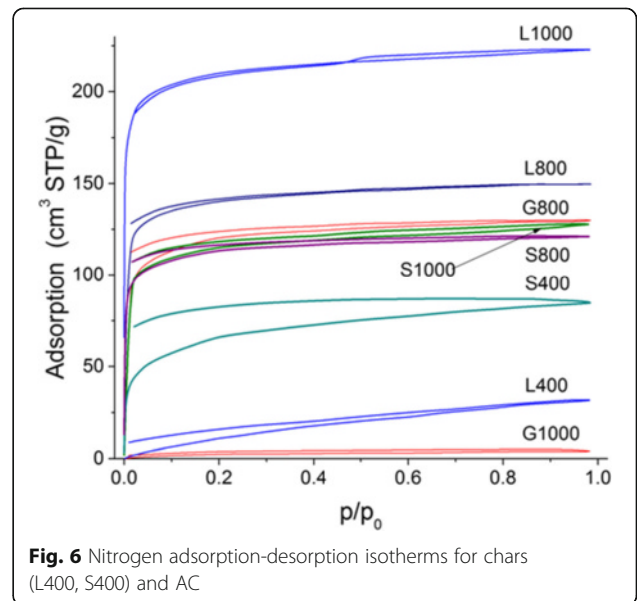
Fig. 6 Nitrogen adsorption-desorption isotherms for chars (L400, S400) and AC

Myronyuk et al. Nanoscale Research Letters (2016) 11:508

Page 6 of 9

Table 2 Textural characteristics of chars and activated carbons

Sample	Burn-off (%)	ρ_b (g/cm³)	S_{BET} (m²/g)	V_p (cm³/g)	S_{nano} (m²/g)	S_{meso} (m²/g)	V_{nano} (cm³/g)	V_{meso} (cm³/g)	S_{QSDFT} (m²/g)	S_{NLDFT} (m²/g)
G400	42[a]	0.29	185[c]							
G800	22[b]	0.64	383	0.201	181	202	0.086	0.113	334	263
G1000	56[b]	0.60	10	0.006	2	8	0.001	0.005	8	7
L400	42[a]	0.50	62	0.049	2	60	0.001	0.046	39	31
L800	32[b]	0.54	437	0.232	318	119	0.162	0.070	395	318
L1000	46[b]	0.64	652	0.345	497	155	0.226	0.118	714	626
S400	44[a]	0.50	223	0.131	148	75	0.069	0.061	211	166
S800	28[b]	0.77	356	0.187	204	152	0.092	0.095	353	280
S1000	42[b]	0.75	362	0.198	225	137	0.115	0.083	316	241

With respect to the weight of a [a]precursor or a [b]char, ρ_b is the bulk density, [c]the specific surface area was calculated using the SAXS data, and the values of S_{nano}, V_{nano}, S_{meso}, and V_{meso} were calculated using the SCV/SCR method

graphite, these distances correspond to 0.338 and 0.202 nm [1–3]. Thus, increasing in the activation temperature leads to certain ordering of the carbon structure; however, it remains turbostratic [1–3] with increased inter-plate distances in comparison with those in graphite.

The IR spectra of lactose-based carbons (as representatives) show (Fig. 3) certain changes in the composition of the material during partial oxidizing (activation) at 1000 °C. For L400, the bands at 579, 1490, and 1600 cm⁻¹ correspond to different vibrations of the CC bonds in the aromatic rings [52–54]. For L1000, these bands shift to 594, 1555, and 1632 cm⁻¹ that correspond to certain ordering of the structure and a decrease in the CC bond length. Some bands (1388, 667, 2349 cm⁻¹) correspond to vibrations in CO_2 [52–56] bound to the carbons. For L1000, an intensive band $\nu_3 = 2343$ cm⁻¹ and less intensive band $\nu_1 = 1381$ cm⁻¹ shift toward lower wavenumbers in contrast to the band $\nu_2 = 672$ cm⁻¹. This corresponds certain changes in the surroundings of the mentioned
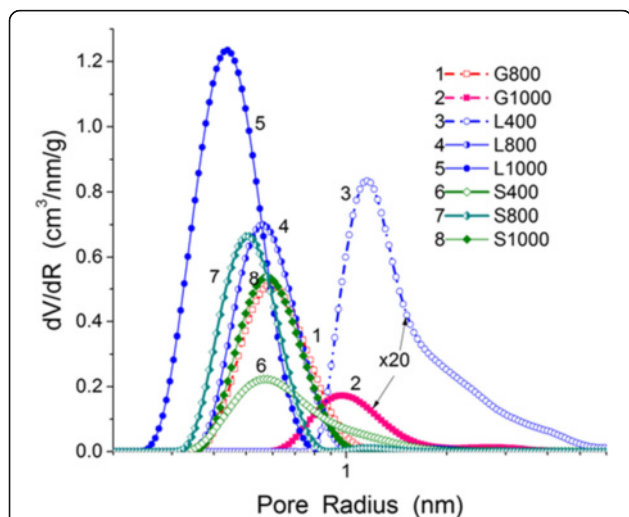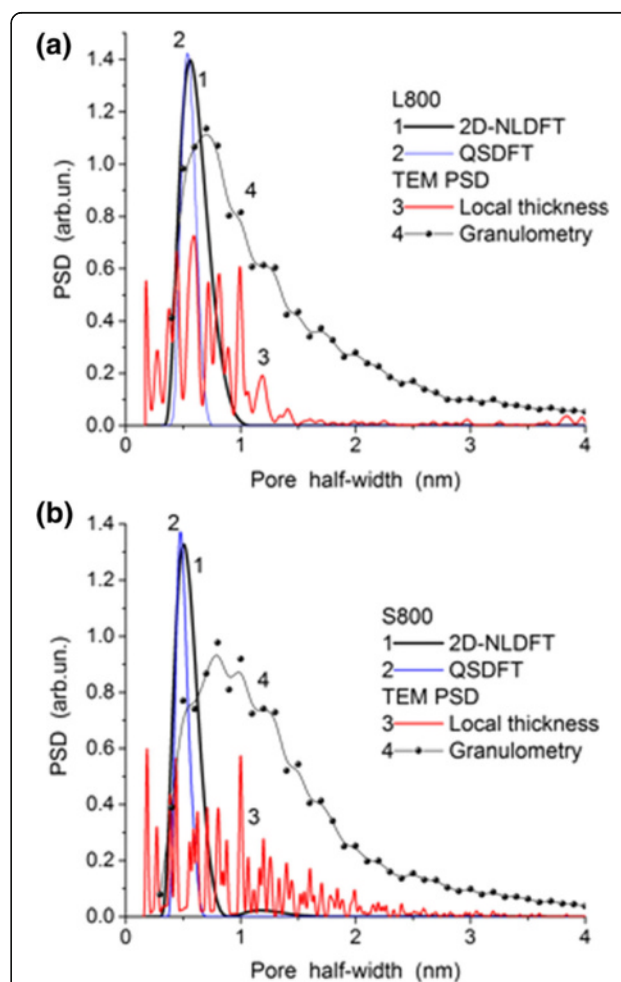

Fig. 8 Pore size distributions of L800 (**a**) and S800 (**b**) calculated using the 2D-NLDFT and QSDFT methods with the slit-shaped pore model and TEM images (Fig. 6a, c) treated using Fiji (local thickness plugin) and ImageJ (granulometry plugin) software
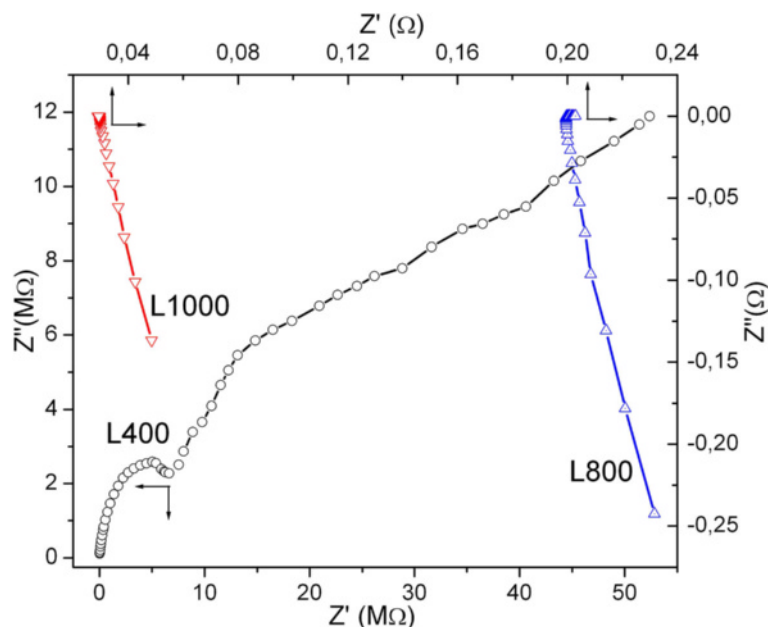

Fig. 7 Pore size distributions calculated using the 2D-NLDFT method with the slit-shaped pore model

Myronyuk *et al. Nanoscale Research Letters* (2016) 11:508

Page 7 of 9

Fig. 9 Nyquist plots for lactose-based char (L400) and activated carbons (L800 and L1000)

structures during oxidizing activation with increasing temperature. The bands at 1712 and 782 cm^{-1} (L400) and 1703 and 790 cm^{-1} (L1000) correspond to the vibrations of the >C=O bonds (C is located in the aromatic ring). A broad band at 1121–1184 cm^{-1} corresponds to the C–O stretching vibrations [53, 54]. As mentioned above, there are the bands corresponding to the O–H (~3450 cm^{-1}) and C–H (2924–2916 and 2868 cm^{-1}) stretching vibrations of the functionalities bound to carbons. Some of them can be located in closed pores or in places poorly accessible for oxygen (similar to nitrogen molecules, Fig. 6). Therefore, they were not removed during oxidizing activation.

Char L400 is practically nonconducting (Fig. 9) because the values of both real (Z') and imaginary (Z'') components of the impedance (Z^*) are high. The main component of the value of Z'' is the capacitive reactance caused by the barrier capacity at the boundary of carbon particles and the capacity of particles per se [57]. The main reason of this result for L400 is incomplete carbonization to form pure carbon matter. Oxidizing activation of the char at 800or 1000 °C leads to a significant decrease in the resistance (Fig. 9), and the inductive impedance appears instead of the capacitance in the high-frequency range. This is due to a decrease in the content of surface functionalities and the formation of well-ordered carbon sheets. Calculations of real (σ') and imaginary (σ'') components of the complex conductivity (σ^*) vs. frequency (f) show that the values of σ' are greater by two to three orders of magnitude than that of σ'' at $f <$ 1 kHz. Estimation of the specific conductivity as the value

of σ^* at $f \rightarrow 0$ (using the plot of σ^* vs. log$f$) (Table 3) shows an increase in the conductivity with increasing temperature of char activation from 800 to 1000 °C because of the ordering of carbon sheets and a decrease in the content of O- and H-containing functionalities discussed above. Lactose-based carbons, which are most porous (Table 2), demonstrate a greater conductivity than other carbons (Table 3). This can be explained by a deeper treatment of the lactose-based carbons with removal of the O- and H-containing functionalities. Additionally, the DTA curve for lactose has the shape different from that for glucose and saccharose over a broad temperature range of 400–1000 °C (Fig. 1).

Conclusions

Thermolysis of glucose, lactose, and saccharose in the inert atmosphere results in the mass loss up to 88% (saccharose), 84.3% (glucose), and 82.9% (lactose) during heating to 1000 °C. Chars prepared at 400 °C contain different O- and H-containing functionalities, whose amounts decrease during oxidizing activation at 800 and 1000 °C. However, according to the IR spectra, certain amounts of these functionalities remain even after heating at 1000 °C in the inert atmosphere. During

Table 3 Specific conductivity (Ω^{-1} m^{-1}) of activated carbons

Precursor	Activation at 800 °C	Activation at 1000 °C
Glucose	6.3	32.2
Saccharose	12.5	61.2
Lactose	58.0	147.5

Myronyuk *et al. Nanoscale Research Letters* (2016) 11:508

Page 8 of 9

heating of the chars in vacuum in the TPDMS experiments, desorption of O- and H-containing fragments is maximal at ~300 °C.

Oxidizing activation of the chars with controlled amounts of oxygen penetrating into the closed vessels through nanosized pores results in an increase in the porosity and specific surface area of carbons depending on the type of the used precursors. The maximum enhanced porosity is observed for lactose-based carbon activated at 1000 °C. For saccharose-based carbon, the difference in the porosity of samples activated at 800 and 1000 °C is relatively small. For glucose-based carbon, a very strong decrease in the porosity is observed for carbon activated at 1000 °C.

All carbons have nanopores and narrow mesopores; broad mesopores and macropores are practically absent. The hysteresis loops of the nitrogen adsorption-desorption isotherms are open for all chars and carbons with one exception of lactose-based carbon L1000 activated at 1000 °C and possessing the maximal values of V_p and S_{BET}. These results can be explained by burn-off mainly of the outer layers of carbon particles and a small degree of burn-off in pores. The second process is maximal for L1000 as the most porous sample studied. An increase in the activation temperature leads to an increase in the conductivity of carbons that is maximal for L1000. This can be explained by deeper activation of this carbon and more effective removal of the O- and H-containing functionalities.

Additional file

Additional file 1: Figures S1 and S2. Show electron diffraction patterns and pore size distributions of activated carbons. **Figure S1.** Electron diffraction patterns for samples (a) L800 and (b) S800. **Figure S2**. Pore size distributions calculated using the SCV/SCR method and TEM images treated using ImageJ with the granulometry plugin. (DOCX 400 kb)

Abbreviations
2D-NLDFT: 2D-nonlocal density functional theory; AC: Activated carbon; BET: Brunauer-Emmett-Teller; DTA: Differential thermal analysis; DTG: Differential thermogravimetry; IR: Infrared; PSD: Pore size distribution; QSDFT: Quenched solid density functional theory; SCR: Self-consistent regularization; TEM: Transmission electron microscopy; TG: Thermogravimetry; TPDMS: Temperature-programmed desorption mass-spectroscopy; XRD: X-ray diffraction

Authors' Contributions
IFM performed the problem definition, analyzed the IR-spectra and TEM images, and participated in the discussion of the experimental results. VIM stated the choice method and subjects of investigation; performed the XRD, low-temperature porometry, and impedance spectroscopy experiments; and participated in the analysis and interpretation of the data. VMS fabricated the initial standards and performed TG/DTG/DTA the experiment. VMG calculated the porous structure parameters of explored standards, analyzed the XRD and TPDMS spectra, participated in the analysis and interpretation of data, and wrote the paper. All authors read and approved the final version.

Authors' Information
IFM is the Head of the Organic and Analytical Chemistry Department and a senior researcher at Vasyl Stefanyk PreCarpathian National University, Ivano-Frankivsk, Ukraine. VIM is an associate professor at the Physics and Technology Department, Vasyl Stefanyk PreCarpathian National University, Ivano-Frankivsk, Ukraine. VMS is a research assistant at the Organic and Analytical Chemistry Department, Vasyl Stefanyk PreCarpathian National University, Ivano-Frankivsk, Ukraine. VMG is a Professor and Head of the Department of Amorphous and Structurally Ordered Oxides, Chuiko Institute of Surface Chemistry, Kyiv, Ukraine.

Competing Interests
The article contains no information which would touch the personal or financial interests of other people and organizations.

Author details
[1]Vasyl Stefanyk Precarpathian National University, 57 Shevchenko Street, 76018 Ivano-Frankivsk, Ukraine. [2]Chuiko Institute of Surface Chemistry, 17 General Naumov Street, 03164 Kyiv, Ukraine.

References
1. Bansal CR, Donnet JB, Stoeckli F (1988) Active carbon. Marcel Dekker, New York
2. Smisek M, Cerny S (1970) Active carbon. Elsevier, Amsterdam
3. Xie Z-L, White RJ, Weber J, Taubert A, Titirici MM (2011) Hierarchical porous carbonaceous materials via ionothermal carbonization of carbohydrates. J Mater Chem 21:7434–7442.
4. Huang S, Shi J (2014) Monolithic macroporous carbon materials as high-performance and ultralow-cost sorbents for efficiently solving organic pollution. Ind Eng Chem Res 53:4888–4893
5. Nowicki P, Skrzypczak M, Pietrzak R (2010) Effect of activation method on the physicochemical properties and NO₂ removal abilities of sorbents obtained from plum stones (Prunus domestica). Chem Eng J 162:723–729
6. Yagmur E, Ozmak M, Actas Z (2008) A novel method for production of activated carbon from waster tea by chemical activation with microwave energy. Fuel 87:3278–3285
7. Lv Y, Gan L, Liu M, Xiong W, Xu Z, Zhu D, Wright DS (2012) A self-template synthesis of hierarchical porous carbon foams based on banana peel for supercapacitor electrodes. J Power Sources 209:152–157
8. Lee J, Yoon S, Hyeon T, Oh SM, Kim KB (1999) Synthesis of a new mesoporous carbon and its application to electrochemical double-layer capacitors. Chem Commun 21:2177–2178
9. Byrne CE, Nagle DC (1997) Carbonization of wood for advanced materials applications. Carbon 35:259–266
10. Falco C, Marco-Lozar JP, Salinas-Torres D, Morallón E, Cazorla-Amorós D, Titirici MM, Lozano-Castelló D (2013) Tailoring the porosity of chemically activated hydrothermal carbons: influence of the precursor and hydrothermal carbonization temperature. Carbon 62:346–355
11. Fuertes AB, Sevilla M (2015) High-surface area carbons from renewable sources with a bimodal micro-mesoporosity for high-performance ionic liquid-based supercapacitors. Carbon 94:41–52
12. McEnaney B (2002) Carbonization and graphitization. Phys Technol 5:5–7
13. Marsh H, Rodríguez-Reinoso F (2006) Activated carbon. Elsevier, London
14. Yu JS, Yoon SB, Chai GS (2001) Ordered uniform porous carbon by carbonization of sugars. Carbon 39:1442–1446
15. Lee JW, Kwon TO, Moon IS (2004) Adsorption of monosaccharides, disaccharides, and maltooligosaccharides on activated carbon for separation of maltopentaose. Carbon 42:371–380
16. Sevilla M, Sanchís C, Valdés-Solís T, Morallón E, Fuertes AB (2008) Direct synthesis of graphitic carbon nanostructures from saccharides and their use as electrocatalytic supports. Carbon 46:931–939
17. Ryu J, Suh YW, Suh DJ, Ahn DJ (2010) Hydrothermal preparation of carbon microspheres from mono-saccharides and phenolic compounds. Carbon 48:1990–1998
18. Lee JS, Mayes RT, Luo H, Dai S (2010) Ionothermal carbonization of sugars in a protic ionic liquid under ambient conditions. Carbon 48:3364–3368

Myronyuk *et al. Nanoscale Research Letters* (2016) 11:508

Page 9 of 9

19. St. Dennis JE, Venkataraman P, He J, John VT, Obrey SJ, Currier RP, Lebrón-Colón M, Sola FJ, Meador MA (2011) Rod-like carbon nanostructures produced by the direct pyrolysis of α-cyclodextrin. Carbon 49:718–722

20. Narasimman R, Prabhakaran K (2012) Preparation of low density carbon foams by foaming molten sucrose using an aluminium nitrate blowing agent. Carbon 50:1999–2009

21. Narasimman R, Prabhakaran K (2012) Preparation of carbon foams by thermo-foaming of activated carbon powder dispersions in an aqueous sucrose resin. Carbon 50:5583–5593

22. Kalijadis A, Đorđević J, Trtić-Petrović T, Vukčević M, Popović M, Maksimović V, Rakočević Z, Laušević Z (2015) Preparation of boron-doped hydrothermal carbon from glucose for carbon paste electrode. Carbon 95:42–50

23. Romero-Anaya AJ, Ouzzine M, Lillo-Ródenas MA, Linares-Solano A (2014) Spherical carbons: synthesis, characterization and activation processes. Carbon 68:296–307

24. Rouzaud JN, Oberlin A (1989) Structure, microtexture, and optical properties of anthracene and saccharose-based carbons. Carbon 27:517–529

25. Shuttleworth PS, Budarin VL, White RJ, Gun'ko VM, Luque R, Clark JH (2013) Molecular-level understanding of the carbonisation of polysaccharides. Chem Eur J 19:9351–9357

26. Tennison SR (1998) Phenolic resin derived activated carbons. Appl Cat A Gen 173:289–311

27. Gun'ko VM, Kozynchenko OP, Turov VV, Tennison SR, Zarko VI, Nychiporuk YM, Kulik TV, Palyanytsya BB, Osovskii VD, Ptushinskii YG, Turov AV (2008) Structural and adsorption studies of activated carbons derived from porous phenolic resins. Colloids Surf A: Physicochem Eng Aspects 317:377–387

28. Gun'ko VM, Turov VV, Kozynchenko OP, Palijczuk D, Szmigielski R, Kerus SV, Borysenko MV, Pakhlov EM, Gorbik PP (2008) Characteristics of adsorption phase with water/organic mixtures at a surface of activated carbons possessing intraparticle and textural porosities. Appl Surf Sci 254:3220–3231

29. Lillo-Ródenas MA, Cazorla-Amorós D, Linares-Solano A (2003) Understanding chemical reactions between carbons and NaOH and KOH: an insight into the chemical activation mechanism. Carbon 41:267–275

30. Carvalho AP, Gomes M, Mestre AS, Pires J, de Carvalho MB (2004) Activated carbons from cork waste by chemical activation with K_2CO_3: application to adsorption of natural gas components. Carbon 42:672–674

31. Wang H, Zhong Y, Li Q, Yang J, Dai Q (2008) Cationic starch as a precursor to prepare porous activated carbon for application in supercapacitor electrodes. J Phys Chem Solids 69:2420–2425

32. Rodriguez-Reinoso F, McEnaney B, Rouquerol J, Unger K (eds) (2002) Studies in surface science and catalysis. Vol. 144. Characterisation of porous solids VI. Elsevier Science, Amsterdam

33. Armandi M, Bonelli B, Geobaldo F, Garrone E (2010) Nanoporous carbon materials obtained by sucrose carbonization in the presence of KOH. Micropor Mesopor Mater 132:414–420

34. Shcherban ND, Ilyin VG (2015) Matrix and bulk synthesis, activation and functionalization of nanoporous carbon adsorbents. Chem Phys Technol Surf 6:97–121

35. Garrett RH, Grisham CM (2005) Biochemistry, 3rd edn. Thomson Brooks/Cole, Belmont

36. Bochkov AF, Afanasyev VA, Zaikov GE (1980) Carbohydrates. Nauka, Moscow

37. Anslyn EV, Dougherty DA (2006) Modern physical organic chemistry. University Science, Sausalito

38. Gun'ko VM, Leboda R (2002) Carbon-silica gel adsorbents. In: Hubbard AT (ed) Encyclopedia of surface and colloid science. Marcel Dekker, New York, pp 864–878

39. Skubiszewska-Zięba J, Leboda R, Seledets O, Gun'ko VM (2003) Effect of preparation conditions of carbon-silica adsorbents based on mesoporous silica gel Si-100 and carbonised glucose on their pore structure. Colloids Surf A: Physicochem Eng Aspects 231:39–49

40. Gor GY, Thommes M, Cychosz KA, Neimark AV (2012) Quenched solid density functional theory method for characterization of mesoporous carbons by nitrogen adsorption. Carbon 50:1583–1590.

41. Jagiello J, Olivier JP (2013) 2D-NLDFT adsorption models for carbon slit-shaped pores with surface energetical heterogeneity and geometrical corrugation. Carbon 55:70–80

42. Jagiello J, Ania CO, Parra JB, Cook C (2015) Dual gas analysis of microporous carbons using 2D-NLDFT heterogeneous surface model and combined adsorption data of N_2 and CO_2. Carbon 91:330–337

43. Gun'ko VM (2014) Composite materials: textural characteristics. Applied Surface Sci 307:444–454

44. Fiji. http://pacific.mpi-cbg.de/wiki/index.php/Main_Page. Accessed Aug 2015

45. Gun'ko VM, Kozynchenko OP, Tennison SR, Leboda R, Skubiszewska-Zieba J, Mikhalovsky SV (2012) Comparative study of nanopores in activated carbons by HRTEM and adsorption methods. Carbon 50:3146–3153

46. Prodanov D. http://rsb.info.nih.gov/ij/plugins/granulometry.html. Accessed Aug 2015

47. Pokrovsky VA, Chuiko AA (2001) Temperature-programmed desorption mass spectrometry and features non-isometric reactions on the surface of dispersed solids. In: Chuiko AA (ed) The chemistry of silica surface, vol 1, UkrINTEI, Kiev, Part., pp 79–116

48. Kulyk TV, Palyanytsya BB, Galagan NP (2003) Molecular self-organization in nanosized particles-carbohydrates systems. Nanosystems Nanomaterials Nanotechnologies 1:681–690

49. Abdullah MH, Yusoff AN (1996) Complex impedance and dielectric properties of an Mg-Zn ferrite. J Alloy Comp 233:129–135

50. Gregg SJ, Sing KSW (1982) Adsorption, surface area and porosity, 2nd edn. Academic, London

51. Ostafiychuk BK, Mandzyuk VI, Kulyk YO, Nagirna NI (2014) SAXS investigation of nanoporous structure of thermal-modified carbon material. Nanoscale Res Lett 9:1–6

52. Russo C, Stanzione F, Tregrossi A, Ciajolo A (2014) Infrared spectroscopy of some carbon-based materials relevant in combustion: qualitative and quantitative analysis of hydrogen. Carbon 74:127–138

53. Zawadzki J (1988) Infrared spectroscopy in surface chemistry of carbons. In: Thrower PA (ed) Chemistry and physics of carbon, vol 21. Dekker, New York, pp 147–380

54. Bellamy LJ (1975) The infra-red spectra of complex molecules, 3rd edn. Chapman and Hall, London

55. Gómez-Serrano V, Piriz-Almeida FN, Durán-Valle CJ, Pastor-Villegas J (1999) Formation of oxygen structures by air activation. A study by FT-IR spectroscopy. Carbon 37:1517–1528

56. Fanning PE, Vannice MA (1993) A DRIFTS study of the formation of surface groups on carbon by oxidation. Carbon 31:721–730

57. Biniak S, Swiatkowski A, Pakula M (2001) Electrochemical studies of phenomena at active carbon-electrolyte solution interfaces. In: Radovic LR (ed) Chemistry and physics of carbon, vol 27. Marcel Dekker Inc, New York, pp 125–225